Denoising Electromagnetic Sensor Spectra for Maize Crop Evaluation: A Comparative Study of Advanced Architectures

Paulo E. Cruvinel[1,2]
[1]Embrapa Instrumentation, São Carlos, SP, Brazil
[2]Post-Graduation Program in Computer Science - Federal University of São Carlos, SP, Brazil
Email: paulo.cruvinel@embrapa.br

Abstract— **Precision agriculture relies on high-fidelity data for optimal crop management. However, multispectral sensors mounted on Unmanned Aircraft Systems (UAS) are susceptible to significant electromagnetic noise—including thermal, sensor-specific, and motion-induced sources—which degrades data quality and classification accuracy. This paper addresses the critical issue of denoising electromagnetic sensor spectra, particularly across the visible RED, and Near-InfraRed (NIR) bands. We present a comparative analysis of four denoising techniques: a 1D Convolutional Neural Network (1D-CNN), a Denoising Convolutional Network (DnCNN), a Convolutional Autoencoder (CAE) implemented in TensorFlow, and a proposed hybrid architecture combining a low-pass analog operational amplifier filter with a CNN-Long Short-Term Memory (CNN-LSTM) network. Performance is evaluated using Mean Relative Error (MRE), Peak Signal-to-Noise Ratio (PSNR), and the Structural Similarity Index Measure (SSIM). Numerical results indicate that while pure deep learning models excel at handling random noise, the proposed hybrid approach provides superior preservation of critical spectral features in the NIR region—crucial for crop stress analysis—while enhancing efficiency by reducing the computational load on the network.**

***Keywords-electromagnetic light-band sensors*; *signal filtering*; *convolutional neural network*; *operational amplifier*; *agricultural sensor*; *intelligent instrumentation*.**

I. INTRODUCTION

Noise in electromagnetic (EM) sensor spectra represents unwanted energy—both internal and external—that obscures the desired measurement signal [1]. It is characterized by Power Spectral Density (PSD) across various frequencies and sets the fundamental limits of sensor sensitivity (often defined as the Noise Equivalent Intensity or Noise Floor). Noise in EM systems is categorized by its origin and spectral characteristics, including thermal noise (Johnson-Nyquist Noise) caused by the random thermal motion of electrons in resistive components, recognized as White Noise (constant amplitude across frequency); flicker noise, which is dominant at low frequencies; shot noise, which arises from the discrete nature of electrons crossing potential barriers (e.g., in junctions); environmental noise (EMI), which occurs due power lines, motors or even from natural signals, like lightning for instance, that couple into the sensor via radiation or conduction; Random Telegraph Noise (RTN), which is related to high-frequency switching between two resistance states due to defects in the sensor's free layer, i.e., common in magnetic sensors. In fact, the noise spectrum of a sensor often shows a high-frequency white noise plateau and a rising noise floor at low frequencies due to noise [2].

Table I shows a summary of noise sources related to electromagnetic sensors.

TABLE I. TYPICAL NOISE SOURCES

Type	*Description*	*Frequency Dependency*
Thermal	Brownian motion of electrons	White (Flat)
Flicker (1/f)	Trap-and-release of charges	Proporcional to 1/f
Shot	Quantized nature of charge	White (at high bias)
Environmental	External EMI (50/60Hz, harmonics, among others)	Varies (Spikes)
Microphonics	Mechanical vibrations	Low frequency

Typical techniques to mitigate noise from the ElectroMagnetic (EM) spectrum, which is closely known as ElectroMagnetic Interference (EMI) reduction or ElectroMagnetic Compatibility (EMC) management, focus on grounding, shielding, filtering, and physical layout optimization. These methods aim to reduce the emission of noise at the source and increase the immunity of devices to external interference, i.e., improving the Signal to Noise Ratio (SNR). In such a context, signal filtering plays an important role, since it is a fundamental process in electrical engineering and signal processing, designed to separate, remove, or enhance specific components of a signal (such as noise, interference, or irrelevant frequencies).

Traditional filtering methods, whether analog or digital, are generally linear and require extensive prior knowledge of noise characteristics, making effective signal separation difficult when signal and noise overlap in the frequency domain [3]. This limitation has motivated the adoption of Convolutional Neural Networks (CNNs) as adaptive, non-linear, data-driven filters that can be optimized based on the specific characteristics of the signal [4]. However, the dynamic nature of real-world environments necessitates retraining these models to maintain error margins within acceptable limits. Data samples used for training can lose their validity over time—a phenomenon known as data decay or obsolescence—which leads to performance degradation as current data deviates from the training distribution, causing concept drift.

Conversely, in complex signal or image processing, a single traditional filter often falls short. CNNs, leveraging multiple hidden layers, automatically extract hierarchical, complex patterns—ranging from low-level features (e.g., edges, peaks) to high-level semantic representations [5]. A CNN applies learned kernels to an input (e.g., a 1D signal or image) to produce a feature map. While this process is analogous to Finite Impulse Response (FIR) filtering, the key advantage is that the weights (kernels) are learned directly from the data through backpropagation rather than being handcrafted.

Therefore, selecting the optimal filter for Signal-to-Noise Ratio (SNR) improvement requires a strict evaluation of advantages and disadvantages, balancing the need for aggressive noise mitigation with the preservation of critical signal features.

In this context, hybrid filter architectures—combining the adaptability of CNNs with the reliability of traditional techniques—represent an emerging paradigm for customized, sensor-driven signal processing that warrants further investigation.

The utilization of multispectral sensors for monitoring maize crops has revolutionized precision agriculture [6], enabling the assessment of chlorophyll content, hydration status, and plant stress through the identification of specific reflectance patterns in the Near-InfraRed (NIR) and red-edge spectral bands. Despite their advantages, images collected by UAS-mounted sensors frequently suffer from electrical and magnetic interference [7].

Electromagnetic noise can arise from atmospheric conditions, sensor electronics, and UAS-motor interferences, often presenting as Gaussian noise or complex artifacts. These noises contaminate the spectral data, leading to incorrect vegetation indexes.

To address the limitations of traditional EMI suppression methods, this paper proposes a hybrid approach combining analog filtering with a CNN. The core novelty lies in a two-stage approach: a low-power analog front-end that provides robust, immediate mitigation of broad-band noise, followed by a post-processing CNN that adapts to the specific, complex features of each light-bands signals.

This combination provides both high-frequency attenuation and intelligent, non-stationary noise handling, surpassing the performance limitations of standard filtering techniques. In fact, traditional noise reduction methods (Gaussian filtering) frequently struggle to differentiate between sensor noise and relevant agricultural spectral signatures. This study evaluates not only Deep Learning-based approaches but also hybrid architecture for processing multispectral data from maize crops.

Furthermore, comparative analyses are conducted using the Mean Squared Error (MSE), Peak Signal-to-Noise Ratio (PSNR), and the Structural Similarity Index (SSIM) metrics, which preserve crucial spatial-spectral information for accurate agricultural diagnostics.

Following this introduction, the remainder of this paper is organized as follows. Section II outlines the materials and methods, including agricultural datasets, feature descriptors, and evaluated noise-filtering architectures. Section III provides a comparative analysis of results based on PSNR, SSIM, and MRE metrics. Finally, Section IV presents the conclusions.

II. MATERIALS AND METHODS

A MicaSense RedEdge-M multispectral camera has been considered and embedded onboard, i.e., using a multirotor UAS, DJI Matrice 100 (Figure 1). The specifications of the multispectral sensors from the Micasense camera are detailed in Table II [8].

To capture the various phenomenological states of the maize, eight distinct imaging flights were carried out [9]. In addition, for the light bands data acquisition protocol, the use of the Ground Control Points (GCP), a high-precision GPS in conjunction with a Real-Time Kinematic (RTK) receiver (i.e., allowing accuracy of ± 1 cm, and a Downwelling Light Sensor (DLS) to allow images' contrast correction due to possible superimposition of clouds in the sky has been considered.

TABLE II. SPECIFICATIONS FOR THE MICASENSE CAMERA

Parameters	Specifications
Weigth	170 g (Including DLS)
Dimensions	9.4 cm × 6.3 cm × 4.6 cm (3.7" × 2.5" × 1.8")
External Power	4.2V−15.8V, 4W nominal, 8W peak
Spectral Bands	Narrowband: Blue, Green, Red, Near-IR
Capture Rate	1 capture per second (per band), 12−bit RAW
Ground Sample Distance (GSD)	5.95 cm/pixel (per band)
Wavelength	Blue (475 nm center ± 20 nm) Green (560 nm ± 20 nm) Red (668 nm center ± 10 nm) Near-IR (840 nm ± 40 nm)

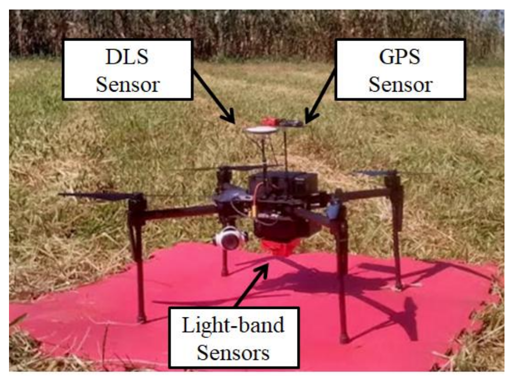

Figure 1. The UAS and hardware setup with sensors for the electromagnetic bands for signals acquisition.

Furthermore, in accordance with the UAS settings and the onboard light-band sensors, for all the flights, the morning periods have been considered to be a time from 11 A.M. to 12 A.M.

To validate the denoising method, for the electromagnetic sensors, when operating in maize crops, an experimental trial was conducted following the cultural management standards of Embrapa Instrumentation. The agricultural experiment took place at the National Reference Laboratory for Precision Agriculture (LANAPRE), in São Carlos, SP, Brazil, near coordinates 21°57'3.9" S and 47°51'10.9" W. The experimental area of 4,000 m² cultivated with maize (Zea mays L.) was managed under precision agriculture principles. As illustrated in Figure 2, the Pioneer P4285 VYHR flat-grain hybrid was used, sown at a density of 5 seeds per linear meter and a spacing of 0.90 m between rows. The layout consisted of forty blocks of 12 rows each (60 rows total), resulting in 600 plants per block and a total population of 24,000 seeds.

Figure 2. Partial view of the maize experimental field during flight 8, taken prior to the critical reproductive stages (silking, blister, dough, dent, and physiological maturity).

The block diagram in Figure 3 illustrates the sensor-based denoising architectures analyzed in this study. Based on data from the multispectral camera, we use both original and filtered signals to evaluate, as an example, the Normalized Difference Vegetation Index (NDVI). The NDVI [10-11] utilizes linear combinations of the RED (668 nm ± 10 nm) and Near Infra-Red (NIR) (840 nm ± 40 nm) bands to monitor biomass density. For agricultural applications, this index is generally analyzed within the 0.0 to 1.0 range.

Besides, prior to calculating the NDVI indices, the analog and digital signals (post A/D conversion) were filtered using several approaches: 1D Convolutional Neural Network (1D-CNN) [12], Denoising Convolutional Neural Network (DnCNN) [13-15], and a Convolutional Autoencoder (CAE) implemented in TensorFlow, CAE (TensorFlow) [16-17]. The performance of these models was compared against a hybrid architecture integrating a active low-pass Butterworth Op-Amp filter [18-19] with a Convolutional Neural Network-Long Short-Term Memory (CNN-LSTM) [20].

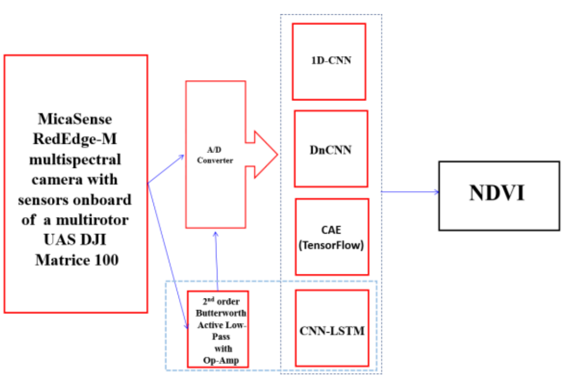

Figure 3. The sensor-based arrangement for the comparative study for denoising the EMI based on advanced architectures.

Regarding the filter`s architecture, the 1D-CNN for Electromagnetic Interference (EMI) noise reduction, it is a deep learning approach that directly analyzes, cleans, and removes unwanted noise from one-dimensional time-series or frequency-domain data. Unlike traditional filtering methods that rely on fixed mathematical transformations, 1D CNNs automatically learn to distinguish between desired signals and noise patterns directly from raw data, resulting in accurate and robust denoising—particularly for complex and non-stationary noise. This specialized network uses convolutional kernels (filters) that slide along a single dimension to extract features. It consists of input layers (for receiving noisy raw data), multiple convolutional layers (for feature extraction), and pooling layers (for down sampling to reduce dimensionality), often structured as an autoencoder that transforms noisy inputs into improved, reconstructed outputs. The network is trained on pairs of noisy and clean signals; through backpropagation, it learns to maximize the SNR and minimize the Mean Squared Error (MSE) between the input and output. In this work, it was implemented as a Convolutional Autoencoder, where the encoder compresses the noisy waveform into a latent representation of key features, and the decoder reconstructs the signal with improvements.

The DnCNN architecture, short for denoising convolutional neural network, is a deep learning-based model designed to remove noise from images (and signals in general) while preserving structural details. Also, unlike traditional denoising methods that often blur images, DnCNN leverages residual learning to specifically learn the noise in an image and subtract it, resulting in sharper and higher-quality outputs.

The core components of DnCNN are centered on residual learning, where the network is trained to learn the residual noise, i.e., the difference between the noisy and an improved image, instead of the direct mapping from noisy to improve the SNR. This approach can allow the training process more efficient and accurate. For this work, we used an architecture that also incorporates batch normalization layers between convolutional layers and rectified linear units, a technique that speeds up training and accelerates convergence. We also used a deep architecture composed of 20 layers of 3x3 convolutions, and pooling layers were intentionally avoided to retain essential structural information.

In addition, a Convolutional Autoencoder (CAE) was implemented in TensorFlow. It serves as a powerful deep learning approach for EMI noise reduction, utilizing unsupervised neural networks to identify, isolate, and remove unwanted electromagnetic noise from captured electronic signals. In this work, the CAE is employed to process digitally converted, noisy EMI signals captured from camera sensors, mapping these corrupted inputs back to a clean, reconstructed state. The architecture consists of an encoder, which uses convolutional layers to compress input signals into a lower-dimensional latent representation, filtering out random noise while retaining essential features,

 ISBN: 978-1-68558-388-0

and a decoder, which reconstructs the denoised signal from this compact representation. Leveraging the TensorFlow framework, the CAE is trained on pairs of noisy and clean data to learn the underlying, noise-free structure of the signal. By focusing on the core signal structure of specific electromagnetic bands, the network learns to ignore high-frequency, chaotic EMI noise. This trained model efficiently removes random noise while preserving crucial signal components. Moreover, a hybrid approach combining a low-pass active Op-Amp filter with a subsequent CNN-LSTM model was implemented for evaluation. This multi-stage strategy leverages hardware speed to eliminate high-frequency noise while using data-driven modeling to remove complex, non-stationary residual interference. The technique operates in two stages: first, an active low-pass analog filter acts as a pre-processing step to reduce broadband EMI, particularly differential-mode noise. Second, the CNN-LSTM model processes the partially filtered signal to remove nonlinear, non-Gaussian, and non-stationary noise that analog filters cannot eliminate. This CNN-based modality extracts spatial-structural features, effectively capturing local temporal-frequency characteristics.

Figure 4 illustrates the second-order Butterworth low-pass filter implemented in this work for each light band. This circuit features a non-inverting Op-Amp configuration with two RC networks to define the frequency response. The corresponding Bode plot demonstrates a characteristic -40 dB/decade roll-off in the stopband. Furthermore, the filter's response is contingent upon the voltage magnification factor (Q) at the cutoff frequency.

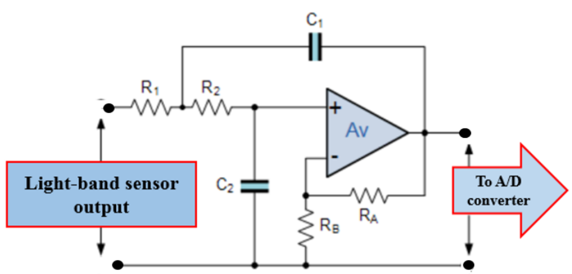

Figure 4. Hardware architecture of the second-order Butterworth low-pass filter used for light-band sensor signal filtering.

The cutoff frequency is given by (1) as follows.

$$f_c = \frac{1}{2\pi\sqrt{R_2 R_3 C_2 C_3}} \tag{1}$$

For the Butterworth response, it is common to set $R_2=R_3$ surface mount resistors and $C_2=C_3$ ceramic capacitor. For a cutoff frequency of 200 kHz with 100 pF capacitors, the resistor value should be equal to 8.2 kΩ. To maintain the Butterworth response (quality factor Q = 0.707) in a Sallen-Key topology of equal components, the Op-Amp gain was fixed at around 1.6 through the feedback resistors. For this work, we have selected the Analog Devices LTC 6269 Op-Amp, which has a 500 MHz Gain-Bandwidth Product (GBW), ultra-low bias current FET-input.

Furthermore, to improve SNR, all the collected signals were filtered, and each ROI was rotated, i.e., taking into consideration the angle calculation by (2) as follows.

$$Rotation = \begin{bmatrix} 1 & 0 & t_x \\ 0 & 1 & t_y \\ 0 & 0 & 1 \end{bmatrix} \begin{bmatrix} \cos\theta & -\sin\theta & 0 \\ \sin\theta & \cos\theta & 0 \\ 0 & 0 & 1 \end{bmatrix} \begin{bmatrix} 1 & 0 & -t_x \\ 0 & 1 & -t_y \\ 0 & 0 & 1 \end{bmatrix} \tag{2}$$

where the parameters ($-t_x$), and ($-t_y$) correspond to the translation of the ROI to the origin, whereas (t_x), and (t_y) can allow shifting it back to its original position.

Additionally, the evaluation of the different filtering processes was conducted using the MSE, PSNR, and the SSIM metrics [21].

The MSE gives a measure about the average of the squares of the errors, which are the differences between corresponding pixel intensities in the original and distorted images. It is given by (3) as follows.

$$MSE = \frac{1}{MN}\sum_{i=1}^{M}\sum_{j=1}^{N}(F(i,j) - I(i,j))^2 \tag{3}$$

The PSNR is the ratio of maximum signal intensity to distortion noise, expressed in decibels (dB). Higher values signify better quality, making it a vital metric for denoising applications requiring high pixel-level precision. It is calculated using (4), with MAX_v defined as the maximum potential pixel value for the given digital image format.

$$PSNR = 20\log_{10}\left(\frac{MAX_v}{\sqrt{MSE}}\right) \tag{4}$$

The SSIM is a perception-based image quality metric that evaluates the similarity between two images (typically an original image and a distorted or noisily image by measuring luminance, contrast, and structural degradation. It is calculated using (5) as follows.

$$SSIM(x,y) = \frac{(2\mu_x\mu_y + c_1)(2\sigma_{xy} + c_2)}{(\mu_x^2 + \mu_y^2 + c_1)(\sigma_x^2 + \sigma_y^2 + c_2)} \tag{5}$$

where μ_x is the pixel sample mean of x, μ_y is the pixel sample mean of y, $(\sigma_x)^2$ is the sample variance of x, $(\sigma_y)^2$ is the sample variance of y, σ_{xy} the sample covariance of x and y, c_1,and c_2 are variables to stabilize the division with weak denominator, i.e. to avoid division by zero. Using SSIM alongside PSNR is crucial because PSNR measures pixel-level technical error (noise removal strength), while SSIM evaluates perceptual structural similarity (edge/detail preservation). PSNR often favors blurry images, whereas SSIM ensures denoised images remain visually clear to human perception, preventing over-smoothing.

III. RESULTS AND DISCUSSIONS

Radiometric calibration was performed previously to the multispectral signal and image acquisition, in fact it was necessary to collect both analog signals from the RED and NIR sensors, as well as to convert then in digital, as metadata, for the digital image to a physical scale.

Besides, the geometry of the aerial image was established by the size of the sensor, the focal length, and the height of the UAS flights, which together determine its Ground Sample Distance (GSD), as presented in Table III. The GSD provides the corresponding measure for the pixels of the surface of the experimental area or the area covered by the image. The percentages established for both the lateral and frontal overlapping of the aerial images were equal to 80% respectively.

The total number of registered images was equal to 320 for each spectral band, i.e., leading to a required storage capacity equal to 14.76 GB (gigabytes), because the surface width and height were equal to 25 m × 80 m, respectively, and the distances between each front and side capture were 4 m and 5 m, respectively.

TABLE III. PARAMETERS USED FOR DATA ACQUISITION

Description	Values	Units
Flying altitude	138	m
Mission flying time	12	min
Max. speed of flying	11	m/s
Front and side overlap	80	%
Ground sample distance	5.95	cm/pixel

Figure 5 shows example results from the eighth flight, featuring rotated images and their corresponding Regions Of Interest (ROI) for block 25 analysis. The images are displayed in RGB, NIR, and RED light-bands, which were used to calculate NDVI values.

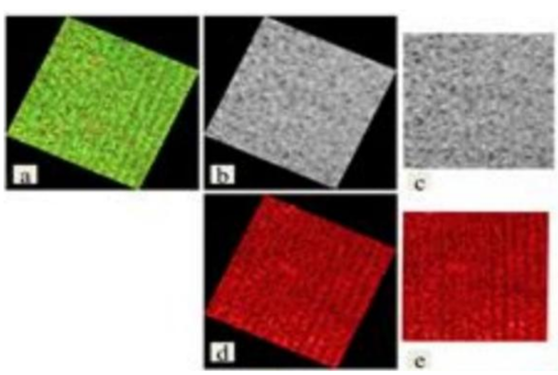

Figure 5. Analysis using the original electromagnetic light-bands (Block 25, Flight 8): (a) RGB, (b) NIR, (c) ROI NIR, (d) RED, and (e) ROI RED.

Table IV presents a numerical comparison of CNN-only architectures versus a hybrid approach that combines a low-pass active filter with a specific CNN algorithm. Utilizing RGB, NIR, and Red light-bands from UAS flight-eight, this analysis evaluates performance in maize crop monitoring using MSE, PSNR, and SSIM metrics.

TABLE IV. NUMERICAL COMPARISON OF CNN-ONLY ARCHITECTURES VERSUS A HYBRID APPROACH

Light-bands	*Metric*	*1D-CNN*	*DnCNN*	*CAE TensorFlow*	*Hybrid Butterworth+ CNN-LSTM*
RED	MRE (%)	5.2	3.5	3;8	1.2
	PSNR (dB)	28.5	32.1	31.5	38.4
	SSIM	0.88	0.92	0.91	0.97
NIR	MRE (%)	6.1	4.0	4.2	1.5
	PSNR (dB)	27.8	31.0	30.5	37.2
	SSIM	0.86	0.90	0.89	0.95

It was possible to observe that the use of the 1D CNN approach for EMI noise reduction is trained on pairs of noisy and less-noisy signals. Through backpropagation, it learns to maximize the SNR and minimize the Mean Squared Error (MSE) between the input and output. It presents high accuracy in removing complex, non-stationary noise. Besides, it does not require handcrafted features or complex pre-processing, operating directly on the raw input data. It is also highly efficient and well-suited for this application and resource-constrained devices. In this work, the 1D CNN was used to invert the EMI data to obtain good images, removing noise from raw data to directly estimate values from agricultural structures.

The use of a DnCNN enabled blind Gaussian denoising, meaning, it was able to remove noise of unknown or varying levels without needing to be retrained for different, specific noise intensities. Such a CNN presents high performance, as it consistently outperforms traditional methods like BM3D in both PSNR and SSIM indices.

By using a Convolutional Autoencoder (CAE) implemented in TensorFlow for noise reduction, it has shown that the model learns to ignore high-frequency, chaotic noise and focus on the core signal structure. In fact, the encoder reduces data dimensionality, essentially filtering out random noise while keeping essential signal components. In the process, the decoder reconstructs the signal without the noise. The observed key benefits include non-linear noise modeling and the processing of complex data, making it useful for application to EMI sources, including those that may occur in agricultural areas.

Furthermore, the proposed hybrid system—utilizing an active 2nd-order Butterworth Op-Amp filter combined with a CNN-LSTM model—outperforms standalone 1D-CNN, DnCNN, and CARE models in denoising and enhancing NDVI across Red and NIR bands. This hybrid architecture provides superior PSNR and SSIM, minimizing the MRE by handling high-frequency noise via hardware (Butterworth filter) and addressing structural/temporal inconsistencies via software (CNN-LSTM). Figure 6 illustrates the resulting application of this hybrid architecture after the filtering process, using a sample from Block 25 of the eight-flight dataset.

For the CNN-LSTM algorithm it was considered convolutional layers to extract the spatial features across each RED, GREEN, BLUE, and NIR light-bands, followed by the LSTM layers to model temporal dynamics and suppress interference. As for all the evaluated CNN in this work, such a model was implemented in Python using an open-source high-level Application Programming Interface (API) to build the neural network (*Keras*), as well as a TensorFlow, where the signal patterns were identified, since LSTM layers learn long-term sequence correlations to refine the signal, using datasets structured as samples, time steps, or even features.

This arrangement has proved to allow a significant impact on the NDVI, as the hybrid model preserves the sharp contrast between RED absorption and NIR reflectance. Figure 7 shows the NDVI maps before the application of the light-bands hybrid filtering process, and after the application of the hybrid filter, i.e., carried out during flight 8, taken prior to the critical reproductive maize stages.

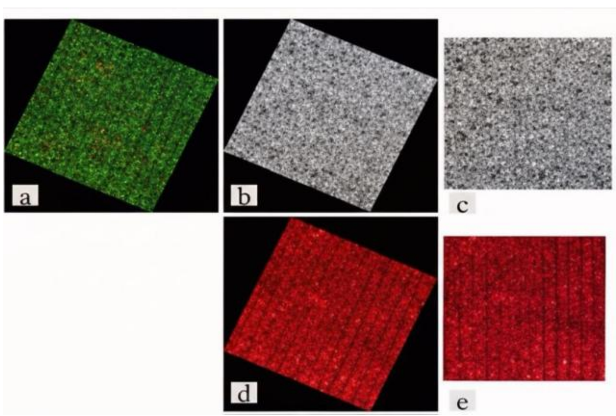

Figure 6. Hybrid architecture filtered samples (Block 25, Flight 8): (a) RGB, (b) NIR(c), ROI for NIR(d), RED(e), and ROI for RED.

Consequently, the resulting NDVI values are closer to ground truth (with less than 0.05 deviation), while standalone models tend to oversmooth, leading to an underestimation of vegetation health and biomass. Working with better-accuracy NDVI values is crucial for maize management because it enables precise, proactive decision-making that optimizes resource use, maximizes yield, and significantly reduces costs. In maize production, small inaccuracies in NDVI can lead to mismanagement of nitrogen fertilizer, incorrect, delayed, or premature irrigation, and an inability to detect early-stage crop stress or nutrient deficiencies before they become irreversible.

In such a context, high-accuracy NDVI allows for variable rate nitrogen application, ensuring fertilizer is applied based on actual plant demand, reducing environmental impact and cost. Also, accurate, time-series NDVI data improves yield predictions, particularly in the mid-to-late growth stages.

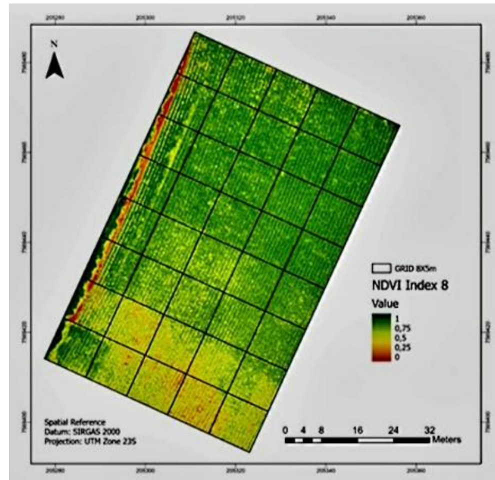

(a)

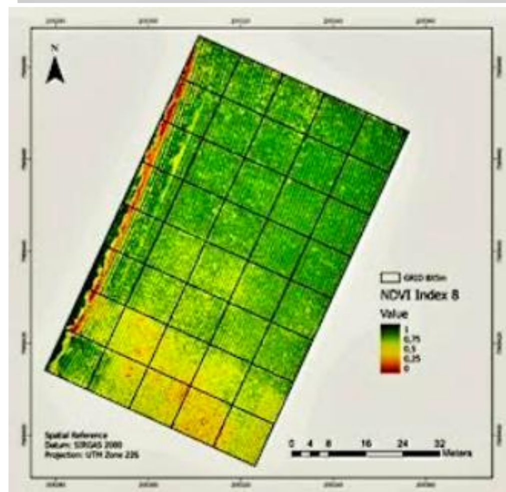

(b)

Figure 7. NDVI maps for the maize experimental field from flight 8, capturing data prior to the critical reproductive stages of the crop. Map (a) shows the results before filtering, while (b) shows the data after applying the hybrid filter for electromagnetic noise reduction.

Furthermore, lower NDVI values can indicate drought, disease, or pest damage. Accurate data acts as an early warning system, allowing farmers to identify stressed zones before they are visible to human being eye.

IV. CONCLUSION AND FUTURE WORK

This work compared 1D-CNN, DnCNN, CAE, and a hybrid CNN-LSTM for spectral denoising across electromagnetic light-bands used in agriculture. The Hybrid CNN-LSTM model provided the best performance, with an average PSNR of 37.8 dB and high SSIM, making it suitable for high-precision, op-amp-based electromagnetic sensor systems. Future research will focus on developing an embedded platform that integrates an active filter and a Convolutional Neural Network (CNN) for real-time agricultural applications, thereby improving crop productivity and optimizing natural resource utilization.

Acknowledgment

This research was partially supported by both the São Paulo Research Foundation, Brazil (FAPESP, Process No. 17/19350-2), and the Brazilian Corporation for Agricultural Research (Embrapa).

References

[1] M. Kaur, S. Kakar, and D. Mandal, “Electromagnetic interference,” in *Proceedings of the 3rd International Conference on Electronics Computer Technology*, Kanyakumari, India, vol. 4, pp. 1-5, 2011.

[2] J T. Kelemenová, O. Benedik, and I. Koláriková, “Signal noise reduction and filtering,” *Acta Mechatronica*, vol. 5, nº. 2, pp. 29-34, 2020.

[3] M. M. Seron and G. C. Goodwin, "Design limitations in linear filtering," in *Proceedings of the 34th IEEE Conference on Decision and Control*, New Orleans, LA, USA, 1995, vol. 2, pp. 1519-1524, 1995.

[4] P. Purwono et al., “Understanding of convolutional neural network (CNN): A review,” *International Journal of Robotics and Control Systems*, vol. 2, nº. 4, pp. 739-748, 2023.

[5] X. Zhao et al., “A review of convolutional neural networks in computer vision,” *Artificial Intelligence Review*, vol. 57, nº.4, pp. 1-43, 2024.

[6] S. Laveglia, G. Altieri, F. Genovese, A. Matera, and G. C. Di Renzo, “Advances in sustainable crop management: integrating precision agriculture,” *AgriEngineering*, vol. 6, nº. 3, pp. 3084-3120, 2024.

[7] P. E. Cruvinel and L. A. Colnago, “Sensor-based platform for evaluation of atmospheric carbon sequestration's potential by maize crops,” in *IARIA, Proceedings of the Tenth International Conference on Advances in Sensors, Actuators, Metering and Sensing (ALLSENSORS 2025)*, Nice, France, pp. 31-36, 2025.

[8] MicaSense RedEdge-M™, Multispectral Camera, *User Manual*, vol. 1, pp. 1-47, 2017.

[9] M. W. L. Carvalho et al., “Productive performance of maize crop irrigated with and without water deficit in different plant arrangements,” *Brazilian Journal of Maize and Sorghum*, vol. 19, pp. 1196-11208, 2020.

[10] J. W. Rouse et al., “Monitoring vegetation systems in the great plains with ERTS,” in Proceedings of the Third Earth Resources Technology Satellite-1 Symposium, National Aeronautics and Space Administration (NASA), SP-351, Washington DC, USA, pp. 309-317, 1974.

[11] C. J. Tucker, “Red and photographic infrared linear combinations for monitoring vegetation,” *Remote Sensing of Environment*, vol. 8, pp. 127-150, 1979.

[12] S. Kiranyaz, O. Avci, O. Abdeljaber, T. Ince, M Gabbouj, and D. J. Inman, “1D convolutional neural networks and applications: A survey,” *Mechanical Systems and Signal Processing*, vol. 151, pp. 107398-107418, 2021.

[13] S. Roy, Single image DnCNN visibility improvement (SImDnCNNVI)”, *Scientific Visualization*, vol. 14, nº. 3, 2022.

[14] X. T. Dong, Y. Li, and B. J. Yang, “Desert low-frequency noise suppression by using adaptive DnCNNs based on the determination of high-order statistic,” *Geophysical Journal International*, vol. 219, nº. 2, pp. 1281-1299, 2019.

[15] T. Rahim, S. Khan, M. A. Usman, and S. Y. Shin, “Exploiting de-noising convolutional neural networks DnCNNs for an efficient watermarking scheme: A case for information retrieval,” *IETE Technical Review*, vol. 38, nº. 2, pp. 245-255, 2021.

[16] Y. Zhang et al., “CAE-CNN: Predicting transcription factor binding site with convolutional autoencoder and convolutional neural network,” *Expert Systems with Applications*, vol. 183, pp. 115404-115414, 2021.

[17] L. Yu, B. Li, and B. Jiao, “Research and implementation of CNN based on TensorFlow,” in *Proceedings of the IOP Conference Series: Materials Science and Engineering*, vol. 490, nº.4, pp. 042022-042027, 2019.

[18] T. Khanna and D. K. Upadhyay, “Design and analysis of higher order fractional step Butterworth filters,” in *Proceedings of the International Conference on Soft Computing Techniques and Implementations (ICSCTI)*, Faridabad, India, pp. 77-82, 2015.

[19] F. S. Ibarra et al., “Design of 2nd order low-pass active filters by preserving the physical meaning of design variables,” *Revista Mexicana de Física*, vol. 57, nº.1, pp. 1-10, 2011.

[20] A. Rostamian and J. G. O’Hara, “Event prediction within directional change framework using a CNN-LSTM model,” *Neural Computing and Applications*, vol. 34, nº. 20, pp.17193-17205, 2022.

[21] D. Sadykova and A. P. James, “Quality assessment metrics for edge detection and edge-aware filtering: A tutorial review,”in Peoceedings of the International Conference on Advances in Computing, Communications and Informatics (ICACCI), pp. 2366-2369, 2017.

 ISBN: 978-1-68558-388-0